

Reconstructing Kernel-based Machine Learning Force Fields with Super-linear Convergence

Stefan Blücher,^{1,2} Klaus-Robert Müller,^{1,2,3,4,5} and Stefan Chmiela^{1,2}

¹*BIFOLD—Berlin Institute for the Foundations of Learning and Data, 10587 Berlin, Germany*

²*Technische Universität Berlin, Machine Learning Group, 10587 Berlin, Germany*

³*Korea University, Department of Artificial Intelligence, Seoul 136-713, Korea*

⁴*Max Planck Institute for Informatics, 66123 Saarbrücken, Germany*

⁵*Google Research, Brain team, Berlin, Germany*

(*Electronic mail: stefan@chmiela.com)

(*Electronic mail: klaus-robert.mueller@tu-berlin.de)

(Dated: 27 December 2022)

Kernel machines have sustained continuous progress in the field of quantum chemistry. In particular, they have proven to be successful in the low-data regime of force field reconstruction. This is because many physical invariances and symmetries can be incorporated into the kernel function to compensate for much larger datasets. So far, the scalability of this approach has however been hindered by its cubical runtime in the number of training points. While it is known, that iterative Krylov subspace solvers can overcome these burdens, they crucially rely on effective preconditioners, which are elusive in practice. Practical preconditioners need to be computationally efficient and numerically robust at the same time. Here, we consider the broad class of Nyström-type methods to construct preconditioners based on successively more sophisticated low-rank approximations of the original kernel matrix, each of which provides a different set of computational trade-offs. All considered methods estimate the relevant subspace spanned by the kernel matrix columns using different strategies to identify a representative set of inducing points. Our comprehensive study covers the full spectrum of approaches, starting from naive random sampling to leverage score estimates and incomplete Cholesky factorizations, up to exact SVD decompositions.

I. INTRODUCTION

In recent years, machine learning force fields (MLFF) have emerged as a valuable modelling tool in quantum chemistry^{1–3}. The promise of MLFFs is to combine the performance of classical force fields with the accuracy of computationally expensive high-level ab initio methods. In this setting, both, neural networks^{4–10} and kernel-based approaches^{11–19} have been successfully applied. To that end, kernel machines are generally considered to be more data efficient in modelling high-quality MLFFs², but yield large linear optimization problems when many training samples and/or large molecule sizes are involved²⁰ (e.g. in materials^{19,21,22} or biomolecules²³). Linear systems are generally solved in closed-form, which has quadratic memory complexity. For large kernel systems, closed-form solutions are therefore not feasible and it is necessary to invoke iterative solvers, which do not require to store the full optimization problem at once^{24–26}. Iterative solvers are highly sensitive to the numerical properties of the underlying system: strong correlations within the data yield ill-conditioned optimization problems that are hard to converge²⁰. MLFFs are exposed to this issue due to stable (non-random) atomic bonding patterns. This is particularly pronounced in models that incorporate differential constraints as inductive bias²⁷. Preconditioners can efficiently capture these correlated structures and thereby separate their effect from the iterative solver. However, their construction relies on the incorporation of physical and chemical domain expertise, as standard approaches do not carry over to the MLFF reconstruction task.

In this study, we discuss the relevant theoretical and prac-

tical considerations necessary to develop the appropriate preconditioner for highly-correlated many-body systems in order to construct accurate FFs. An effective preconditioner has to represent all atomic cross-correlations faithfully, while being computationally cheap to construct. Standard preconditioning approaches, such as Jacobi or sparse preconditioning, remove entries (correlations) from the kernel matrix and are therefore not suitably accurate. The alternative is to use low-rank approximations that compress but, retain all entries in the kernel matrix. The optimal solution would be to find the most relevant subspace spanned by the kernel matrix via SVD decomposition, which is however too expensive. A more economical approach is to approximate the kernel matrix using a limited number of inducing columns. This is the key idea behind the Nyström method²⁸ and the incomplete Cholesky decomposition²⁹, which differ in the way how inducing columns are sampled. These two methods are representative for a broad class of inducing point methods^{29–31} and offer opposing trade-offs with regard to construction cost and convergence speed.

The outline of this study is as follows: Firstly, we motivate and establish all relevant components, which are necessary to build scalable preconditioned kernel solvers. In particular, we provide a comparative discussion for the distinctive properties of inducing column based preconditioners. Secondly, we demonstrate their practical performance, both, in terms of spectral decay as well as actual iterative solver convergence. This leads to an in-depth understanding for the scaling behavior of preconditioned linear solvers and allows us to derive a heuristics to balance computational resources efficiently and thus arrive at accurate FFs.

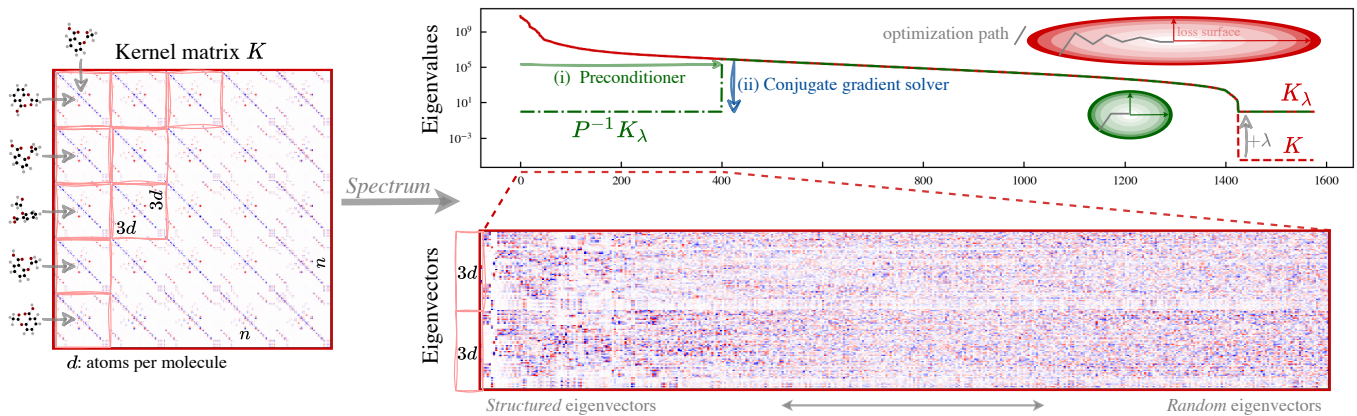


FIG. 1. Left panel: sGMDL kernel for aspirin as a representative example for correlated molecular systems³². Right panel: A preconditioned iterative solver first removes the dominant spectral dimensions and then approximate the remaining spectrum increasingly accurately via a $\#$ -dimensional Krylov subspace ($\#$ iteration steps). Large magnitude differences across eigenvalues lead to narrow valleys in the loss landscape (red ellipse), which obfuscates the optimization path. Preconditioning can remedy this by flattening the spectrum, leading to wider valleys (green roundish ellipse), which are easier to descent. To detail the dominant spectral structure, we focus on the first entries (specifying the contributions of the first two training molecules) of the dominant ~ 400 eigenvectors.

II. SCALABLE KERNEL SOLVERS FOR QUANTUM CHEMISTRY

A. Kernel machines for MLFF

Kernel machines offer a powerful way to model complex functions and have successfully been applied to reconstruct MLFFs^{11–19}. Here, we focus on the symmetric gradient-domain machine learning (sGDML)¹³ model, which incorporates all important invariances of molecular FF to be particularly data efficient¹². The atomic positions are encoded via a descriptor, to obtain a positive semi-definite (PSD) kernel matrix $K \in \mathbb{R}^{n \times n}$ with size $n = 3d n_{\text{train}}$ (n_{train} training molecules with d atoms). The resulting learning problem amounts to solving the regularized linear system

$$K_\lambda \cdot \alpha = y \quad (1)$$

with the kernel $K_\lambda = K + \lambda I_n$ and atomic force labels y . Using the solution α , force predictions for new input conformations can be queried via kernel ridge regression²⁰. Equation (1) is typically solved analytically in closed-form, which requires storage of the full matrix at a memory complexity of $\mathcal{O}(n^2)$ and cubic runtime cost $\mathcal{O}(n^3)$. Following this approach, memory complexity is the bottleneck and prevents scalability to large system sizes or numbers of training points. Iterative solvers can overcome these limitations by solving the optimization problem numerically using gradient descent, which only relies on evaluations of matrix-vector products^{20,24,26,33–37}. The restriction to matrix-vector products remedies the memory constraint as no matrix needs to be stored explicitly^{38,39}. Since K is PSD, the linear system can be solved with the conjugate gradient (CG) algorithm, which is more efficient than plain gradient descent³⁴. The CG iteratively constructs a Krylov subspace based on the current residual (approximation error) and enforcing conjugacy with respect to all previous search directions. This leads to efficient

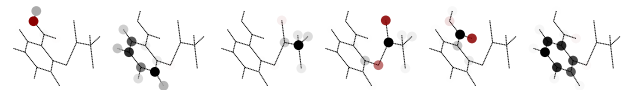


FIG. 2. Atomic contributions per eigenvector (see Appendix A) via marginalizing the molecular periodicity and measuring the spatial L2 distance. The kernel induces a low-rank decomposition, which forms the basis for a prototype molecule.

steps towards the solution α , with a theoretically guaranteed convergence in (at most) linear $\# \leq n$ time, i.e., $\mathcal{O}(\#n^2)$. Depending on the spectral properties of the kernel matrix, super-linear convergence in $\# \ll n$ is often achieved in practice^{40–42}. In particular, the condition number (ratio of largest to smallest singular value) and the characteristic eigenvalue decay is decisive for the overall performance of this algorithm.

To illustrate this, we discuss these spectral properties for a specific example that is representative for the molecular datasets considered in this work (see Figure 1, left panel) and most correlated systems in general. The kernel matrix consists of $(3d \times 3d)$ block matrices, which correspond to pairwise correlations between two training molecules. Each block represents the correlation structure between the d atoms within each example. The molecular structures are restricted by the laws of quantum chemistry, which yields similar spectral characteristics across different systems. This enables us to derive transferable numerical insights about the kernel-based force field reconstruction problem. The eigenvectors and eigenvalues are shown in red (right panel of Figure 1). For clarity, we only show the dominant 400 eigenvectors (columns) and their entries corresponding to two molecule (rows). The dominant eigenvectors exhibit a periodic pattern, which can be interpreted as a small set of prototypical molecular block structure elements. These patterns represent atom-wise contributions by each eigenvector (see Appendix A for details), which

we visualize in Figure 2. Intuitively, the structured eigenvectors form a low-rank basis for the full molecule, as they capture recurring sub-structures across all training points, e.g., strong correlations between interacting atoms. On the other hand, the remaining low-magnitude eigendirections represent high-frequency fluctuations from the prototypical geometries. These eigenvectors contribute the individual geometric features of the training data⁴³. This part of the spectrum decreases less rapidly, compared to the dominant part of the spectrum. We denote this as the spectral plateau phase. The spectrum also includes a (regularized) null space, which is unavoidable, due to a roto-translationally invariant representation of the molecule in terms of pairwise distances.

B. Theoretical preconditioning for MLFF

The large differences in magnitude across eigenvalues (large condition number) induce long and narrow multi-dimensional valleys along the loss surface. These narrow valleys hamper gradient descent solvers, since the optimization path bounces back and forth on the way to the solution (see ellipses in Figure 1). A suitable preconditioner is a full-rank matrix $P \approx K_\lambda$ that captures the dominant spectral components, allowing for a partial normalization to effectively smoothen the underlying loss landscape^{36,44–49}. Accordingly, the linear system can equivalently be reformulated as

$$P^{-1}K_\lambda \cdot \alpha = P^{-1}y, \quad (2)$$

which preserves the original solution α , but has improved numerical properties that lead to a faster iterative convergence. To retain the original PSD structure, we require that a symmetric decomposition $P = LL^T$ ($L \in \mathbb{R}^{n \times n}$) exists^{20,44,46}.

Another key requirement is that the construction of the preconditioner P should not dominate the overall computational costs. Generally, there are two principled ways to achieve this⁵⁰: Either via sparsification of the kernel matrix (e.g. zero-out entries to obtain a block-diagonal form) or via a compression into a low-rank representation. Only the latter approach is able to faithfully represent the complex correlation structure of quantum chemical systems. In this work, we therefore focus on symmetric low-rank approximations $K \approx K_k = L_k L_k^T$ ($L_k \in \mathbb{R}^{n \times k}$, $k \ll n$), which are supplemented into full-rank preconditioners after the regularization term is added:

$$P = L_k L_k^T + \lambda I_n. \quad (3)$$

Its inverse P^{-1} can be computed economically via the Woodbury formula²⁰:

$$P^{-1} = \lambda^{-1} [I_n - L_k (\lambda I_k + L_k^T L_k)^{-1} L_k^T]. \quad (4)$$

The runtime of this approach is given by $\mathcal{O}(k^2 n)$ and can be implemented symmetrically based on a single matrix $\mathbb{R}^{n \times k}$ ²⁸, which limits the memory complexity to $\mathcal{O}(kn)$.

Theoretically, the optimal rank- k approximation K_k is given by the singular-value decomposition (SVD). Since K is PSD the singular values are given by the squared eigenvalues and

the SVD is identical to the eigenvalue decomposition. Based on these eigenvectors, a *SVD preconditioner* can directly remove the k dominant eigenvalues and hence, optimally flatten the spectrum (green arrow in Figure 1). The remaining spectrum is then iteratively approximated within the Krylov subspace generated by the CG algorithm (blue arrow in Figure 1). Overall, this leads to a complete decomposition of the kernel, see Appendix A for a technical formulation of this argument.

Since, every eigenvector is build up by a unique linear combination of kernel columns, it requires access to all columns to construct the SVD. Hence, the SVD is too expensive $\mathcal{O}(kn^2)$ and only useful as a theoretical lower bound for the performance of a practical rank- k preconditioners. For the same reason random projection methods^{51,52}, which combine multiple columns into a single vector, are also not possible and we need to directly rely on the span of kernel columns (Section III).

III. NYSTRÖM APPROXIMATION

A low-rank approximation of the kernel matrix can be constructed as a projection onto a subset of its columns. This idea forms the basis behind the Nyström method. Traditionally, it is employed to approximate large scale kernel machines^{28,31,53–57} and recently also as a preconditioner^{46,58–60}. If we are given $k \ll n$ inducing columns $K_{nk} = \begin{pmatrix} K_{kk} \\ K_{(n-k)k} \end{pmatrix}$, the Nyström approximation expresses the full kernel matrix according to

$$K \approx K_k = K_{nk} K_{kk}^{-1} K_{nk}^T = \begin{pmatrix} K_{kk} & K_{(n-k)k}^T \\ K_{(n-k)k} & K_{(n-k)k} K_{kk}^{-1} K_{(n-k)k}^T \end{pmatrix}. \quad (5)$$

Here, the matrix dimensionality is implicitly encoded in the subscript, i.e., $K_{(n-k)k} \in \mathbb{R}^{(n-k) \times k}$. The K_{kk} can be symmetrically factorized to obtain the form in Equation (3), see^{20,61} for implementation details. The approximation error is given by the Schur complement $S = K/K_{kk} = K_{(n-k)(n-k)} - K_{(n-k)k} K_{kk}^{-1} K_{(n-k)k}^T$. Intuitively, all $(n-k)$ remaining columns are expressed in the basis of the inducing columns. Therefore, the accuracy is highly dependent on selecting the most representative set of inducing columns.

We now set out to find expressive inducing columns for the dominant part of the spectrum, i.e. which are able to capture the low-rank decomposition depicted in Figure 2.

Column sampling strategies

Uniform sampling The simplest approach is to draw a random sample of columns^{28,30,62,63}. This approach is computationally inexpensive and agnostic to the spectral properties of the kernel matrix. It provides a baseline for our study.

Leverage scores Not all columns contribute equally to the composition of the kernel matrix. A random sample of inducing columns does therefore not necessarily provide a good ap-

proximation for the column space spanned by the kernel matrix. To get a better representation, leverage scores can be used to measure how uniformly information is distributed among all columns^{31,64–66}. Columns that are strongly correlated with many others, get assigned a low leverage score, while linearly independent columns mostly represent themselves and yield large leverage scores. Sampling according to leverage scores thus gives a higher chance of recovering a more representative set of inducing columns for the kernel matrix spectrum^{43,67}, although linear independence is not guaranteed.

In our ridge regression setting, it is appropriate to consider *ridge leverage scores* $\tau_i(K) = \left(K(K + \lambda I_n)^{-1}\right)_{ii}$ ^{67,68}, which use a diagonal regularization parameter λ to diminish small components of the kernel spectrum. Here, each kernel column is projected onto the regularized kernel to determine its overlap with the columns of the regularized kernel matrix. To make the computation economical, we need to approximate the ridge leverage scores in practise and follow refs.^{20,67} here.

Incomplete Cholesky Lastly, we discuss the *incomplete Cholesky*^{24,26,61,69} decomposition as sampling strategy. The algorithm constructs a low-rank representation $K_k = L_k L_k^T$, by iteratively selecting inducing columns based on the Schur complement $S \in \mathbb{R}^{(n-1) \times (n-1)}$. In each step, the Schur complement characterizes the approximation error (kernel space not spanned by the inducing columns) of the Nyström method in Equation (5). In the first iteration, we have (inducing column already permuted to the front, i.e., $K_{n1} = \begin{pmatrix} K_{11} \\ \mathbf{b} \end{pmatrix}$):

$$S = K/K_{11} = K_{(n-1)(n-1)} - \frac{1}{K_{11}} \mathbf{b} \mathbf{b}^T. \quad (6)$$

The Schur complement S is used as input for the next Cholesky iteration. Thereby, the effect of all previous inducing columns is accounted for, before choosing the next column. The largest diagonal element of S indicates the next inducing column, by which the approximation error is minimized according to the trace norm⁷⁰. Since the trace is equal to the sum of all eigenvalues, this pivot rule focuses on the columns which are expressive for the current dominant eigendirections. Despite being a greedy approach, the incomplete Cholesky systematically orthogonalizes correlated columns and thereby ensures a set of linearly independent columns, which enhances representative power and improves numerical stability⁶¹. In this way, and in contrast to leverage score sampling, correlated inducing columns are avoided. This leads to close to optimal accuracy in practise and a theoretically guaranteed exponential convergence for sufficiently high exponential eigenvalue decay rates⁷⁰. This procedure can be used as a column sampling scheme, by keeping track of the column index that is removed in each step. Note that, if identical inducing columns are chosen for the incomplete Cholesky algorithm and the Nyström method, both methods are equivalent^{29,30}. However, the incomplete Cholesky algorithm is as costly as the overall preconditioner approach $\mathcal{O}(k^2 n)$ ⁷⁰, whereas the cost for the leverage scores estimation can be readily adapted by the fidelity of the approximation scheme⁶³. We present an efficient implementation in Appendix A 2.

A. Runtime considerations

Previously, we discussed how to build a scalable kernel solver with a column sampling based preconditioner. To mitigate memory constraints and facilitate iterative solvers, an efficient routine for the matrix-vector product of K is required. Secondly, we require a preconditioner to enable super-linear convergence and ease runtime limitations. This preconditioner requires k inducing columns, which are accessible via naive application of the matrix-vector in quadratic costs $\mathcal{O}(kn^2)$. Since this would dominate the overall computational costs, we require an additional routine, which can retrieve (a single or multiple) columns in linear time.

Particularly, sGDML is an interesting example. Here, the smallest processing units are the pair-wise block correlations between two molecules, which is why, k columns cost at least $\mathcal{O}(dkn)$. Consequently, it is beneficial to retrieve all k columns simultaneously. This is trivial for both probabilistic column sampling approaches. In contrary, this is not possible for the incomplete Cholesky decomposition, for which a single column is requested at each iteration step. Consequently, both probabilistic approaches are relatively more efficient. Even though all three approaches are in the same complexity class $\mathcal{O}(k^2 n)$, their computational pre-factors are ordered according to (i) uniform sampling, (ii) leverage scores and (iii) incomplete Cholesky, also see Figure 3.

IV. EXPERIMENTAL RESULTS

Firstly, we consider small kernel systems ($n_{\text{train}} = 250$ for aspirin) in Section IV A and IV B, which allow to benchmark against the optimal SVD preconditioner. In the following Section IV C, we analyse the scaling behavior to large systems and derive a heuristic for a practically well-performing preconditioner size. All datasets and software used in this work are available at www.sgdml.org. Throughout our experiments, we use the sGDML kernel with fixed length scale $\sigma = 10$ and regularization $\lambda = 10^{-10}$.

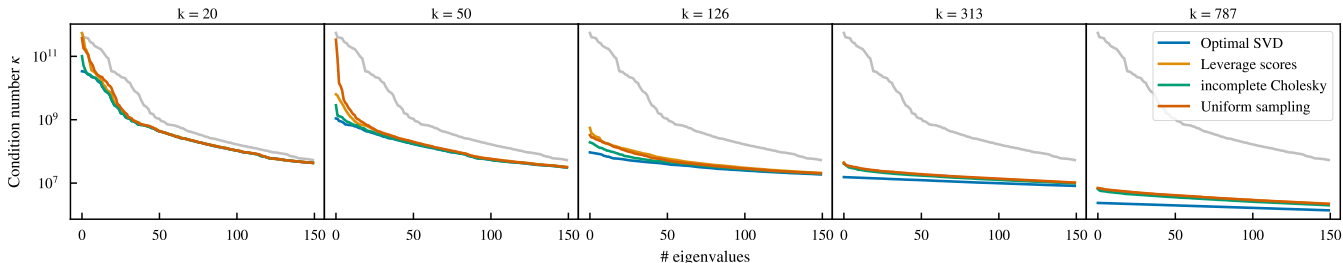
A. Preconditioned spectrum

For iterative solvers, a fast convergence is directly connected to a low condition number of the kernel matrix. We therefore begin our analysis by looking at the spectrum of the preconditioned system $P^{-1}K\lambda$. In Figure 4 we show the 150 dominant eigenvalues for aspirin for various numbers of inducing columns k . As expected from our theoretical considerations, SVD preconditioning is the most effective approach to build a preconditioner, leading to the smallest condition number as compared to all other preconditioner variants in this work. It is worth noting, that superiority of the optimal SVD preconditioner does not surmounted one order of magnitude, independently of the number of inducing columns.

For small numbers of inducing columns, the incomplete Cholesky shows significantly better performance than any



FIG. 3. Relative computational costs of all preconditioners.

FIG. 4. Preconditioned spectrum of $P^{-1}K_\lambda$ for varying preconditioner size k , restricted to the dominant 150 eigenvalues. Results for aspirin ($n_{\text{train}} = 250$, $n = 15750$), more molecules in Appendix B 1. The grey curve corresponds to the original spectrum of K_λ . All practical approaches are lower-bounded by the optimal SVD preconditioner.

of the two column sampling approaches. The incomplete Cholesky decomposition projects out columns through the Schur complement and is therefore able to construct a subspace with approximately orthogonal inducing columns. These inducing columns are therefore more expressive for the eigenvectors revealed by the SVD, than the possibly correlated (less balanced) set of inducing columns returned by the random or leverage score sampling approach. In contrast to SVD, the inducing columns selected by the incomplete Cholesky decomposition are however not guaranteed to match the most important eigendirections, which makes it less effective, yet cheaper to construct.

Since the dominant eigenvectors are partially aligned with the kernel columns, incomplete Cholesky performs nearly optimal for a limited number of inducing columns (up to $k \approx 3d$ in Figure 4). For larger preconditioners this advantage diminishes. Here, the corresponding eigenvectors are not structured and do not align with any kernel column (see lower right panel in Figure 1). Hence, we observe a constant accuracy drop, which is characteristic for the structural discrepancy between kernel column and eigenvectors. This renders the particular column selection less relevant and the preconditioner size k uniquely determines the approximation quality. We observe a similar pattern for other molecules in Appendix B 1. Additionally, we empirically show the limitations of local Jacobi preconditioning^{71–74} in Appendix B 1 and thereby verify the necessity to incorporate all relevant correlations for successful preconditioning.

In summary, all practical preconditioners are lower-bounded by the SVD preconditioning approach. In particular, incomplete Cholesky preconditioning can accurately approximate the structured eigenvectors, which leads to nearly optimal performance for small preconditioners.

B. Convergence speed of conjugate gradient

We quantify the iterative solver runtime by tracking the number of CG steps # until convergence. We choose this performance metric, because it is insensitive to implementation and hardware details. In Figure 5 we show the dependence of convergence speed with respect to the relative preconditioner strength $\frac{k}{n}$. As a representative selection, we present results for four different molecules, which range from small to large molecules: ethanol ($d = 9$), aspirin ($d = 21$), a catcher molecule ($d = 88$) and a large nanotube ($d = 370$)^{20,32} (more molecules in Appendix B 2). The preconditioner strength is varied between $k \sim 50$ up to 14% of all columns.

The grey solid (dashed) horizontal line corresponds to the computational cost of a closed-form solution (10% reduction), which is given by n^3 ($10\% \cdot n^3$). This provides a scale for relative computational complexity. For example, ethanol is simpler (easier to solve), as compared to larger or more complex molecules, such as aspirin. We observe, that the functional dependency between preconditioner strength and computational cost differs between all molecules. In particular, the number of inducing columns necessary to obtain super-linear convergence, depends on the complexity of the molecule. These different complexities are embodied within the characteristic shape of dominant part of the spectrum (see Appendix B 1 for explicit spectra). For example, the catcher molecule requires relatively the most columns, since its spectrum has many degenerate, dominant eigenvalues. Alternatively, for the nanotube further improving the super-linear convergence is the most challenging as compared to all other molecules, since its dominant spectrum is only slowly decaying. In contrast, ethanol is simple to solve and more than 2% preconditioning already lead to rapid convergence (one order of magnitude faster). Generally, too small preconditioners lead to high

computational costs, which are as expensive as the analytic closed-form solution. Contrary, more inducing columns always lead to a faster convergence.

Having discussed commonalities between all approaches, we now analyse their differences with respect to their applicability and numerical performance when applied to different molecules. From Figure 5 it is clear that the SVD preconditioner is the most effective approach. As expected, it lower bounds all other practical preconditioners. Interestingly, the superior performance is not pronounced for small preconditioners but rather independent from the number of inducing columns. Naively, we expect the larger deviations for less inducing columns, as here the optimal eigenvectors are relatively more important. However, the leading dominant eigenvectors are more aligned with kernel columns as compared to sub-dominant eigenvectors (cf. Figure 1), which enables accurate approximations for smaller preconditioners.

Interestingly, all three practical preconditioners perform similarly for most molecules, e.g. consider aspirin in Figure 5, for which barely any difference is visible. We emphasize, that this observation extends to all additional molecules presented in Appendix B 2. Intuitively, this indicates that a uniform subset of columns is expressive for the kernel spectrum and therefore ideally improves the approximation accuracy and hence preconditioner performance. However, both probabilistic column selection methods induces some fluctuation into the preconditioner performance. In contrast, the incomplete Cholesky performance is monotonously improving and does not fluctuate. This is reminiscent of the deterministic pivoting rule, which ensures that the approximation error is always decreasing with increasing number of inducing columns.

Further, we observe noteworthy differences for the larger and more structured catcher and nanotube molecules (two bottom panels in Figure 5). Here, the incomplete Cholesky significantly outperforms both probabilistic column sampling approaches. For small preconditioner sizes the incomplete Cholesky’s performance is close the optimal SVD baseline. For the catcher molecule, this advantage degrades and for larger preconditioners all practical approaches perform equivalently. For the nanotube molecule there are persistent differences between all preconditioner approaches. Here, the performance gap between the SVD preconditioner and both probabilistic approaches increases with the number of inducing columns. This indicates that both approaches do not construct an expressive set of columns. Here, the incomplete Cholesky’s capability to greedily select linear independent columns is decisive, as it allows to targetedly incorporate the relevant molecular structure. Overall, this enables to construct a more representative set of kernel columns.

Lastly, we note, that the leverage score sampling approach is not superior to the uniform sampling baseline, even for small preconditioners ($\sim 2\%$ or $k \sim 300$) in Figure 5. This is counter-intuitive as leverage scores are designed to improve on naive uniform sampling. We speculate that, this is related to the fact that the regularization λ for the ridge leverage scores is fixed and not adapted to changing number of inducing columns k . Hence, ridge leverage scores are indicative for the global spectral properties of the ridge regression task

(K_λ), instead of directly targeting the dominant k -dimensional eigenspace (K_k), which is relevant for preconditioning. We experimentally investigating this intuition in Appendix B 2, via an improved (however computationally costly) notion of leverage scores. These improved leverages scores indeed remove the gap wrt. the uniform sampling baseline. However, they do not improve the preconditioner performance significantly. Therefore, we conclude that the incomplete Cholesky preconditioner is the most capable approach, as it is highly effective in selecting a diverse and representative set of inducing columns. This leads to nearly optimal preconditioning for a large, structured nanotube molecule. However, this relative advantage generally degrades with increasing number of inducing columns. For larger preconditioners it is sufficient to uniformly sample columns, since small eigendirections are less structured as they obtain support from most atoms simultaneously.

C. Optimal number of inducing columns

Next, we investigate the CG’s super-linear advantage, when scaling from smaller to larger kernel systems. To this end, we consider the normalized iteration $\frac{\#}{n}$, which measures the relative advantage of the iterative solver compared to the closed-form solution. A normalized iteration of one indicates equivalent runtimes between both methods. For simplicity we restrict to leverage score preconditioning in the following, which lower bounds the performance of all other practical preconditioners.

In Figure 6 (left panel), we vary the absolute kernel size n and focus on the aspirin molecule. Interestingly, we find that the super-linear advantage does not depend on the kernel size n . It is solely determined by the absolute number of inducing columns k . Hence, there is a constant trade off between iterative solver runtime and memory demand, i.e., for doubling the preconditioner the solver runtime may be halved. This trade off is characterized by a monomial power-law dependence $\frac{\#}{n} \propto k^{-m}$. Here, $m > 0$ can be interpreted as the slope of the linear relation within the log-log space shown in Figure 6.

Next in Figure 6 (right panel), we analyse this trade off for different molecules and fixed kernel size $n = 31400$. We observe, that the monomial relation persists for all molecules. However, offsets and slopes m now depend on the molecule type, as expected from their different spectra (see Appendix B 1). We characterise the offset by the minimal preconditioner size k_{\min} , which indicates parity between iterative and closed-form solver runtime (intersection with solid line). As a consequence, more complex molecules require a larger minimal preconditioner size k_{\min} (see Table I).

Deriving a Rule of Thumb

We now discuss the subtleties of choosing the ideal number of inducing columns k , which minimizes the overall runtime, in advance. Here, we need to balance two extrema: Firstly,

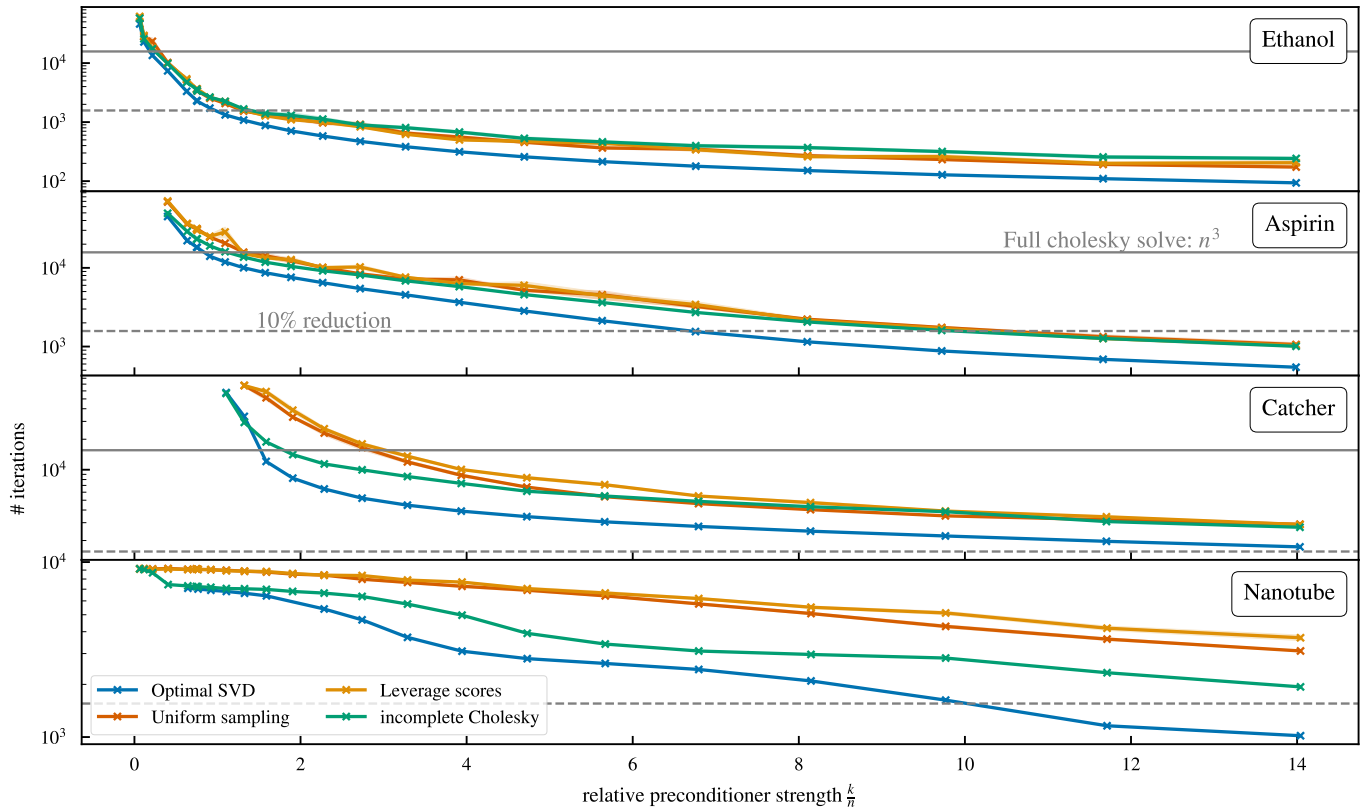


FIG. 5. Iterative convergence speed for varying preconditioner strength for fixed kernel size $n \approx 15000$ ($n_{\text{train}} = 250$ for aspirin). Only minor performance differences are visible for ethanol. In contrast, for more complex molecules (catcher, nanotube) the elaborate incomplete Cholesky preconditioner is superior to probabilistic sampling of inducing columns.

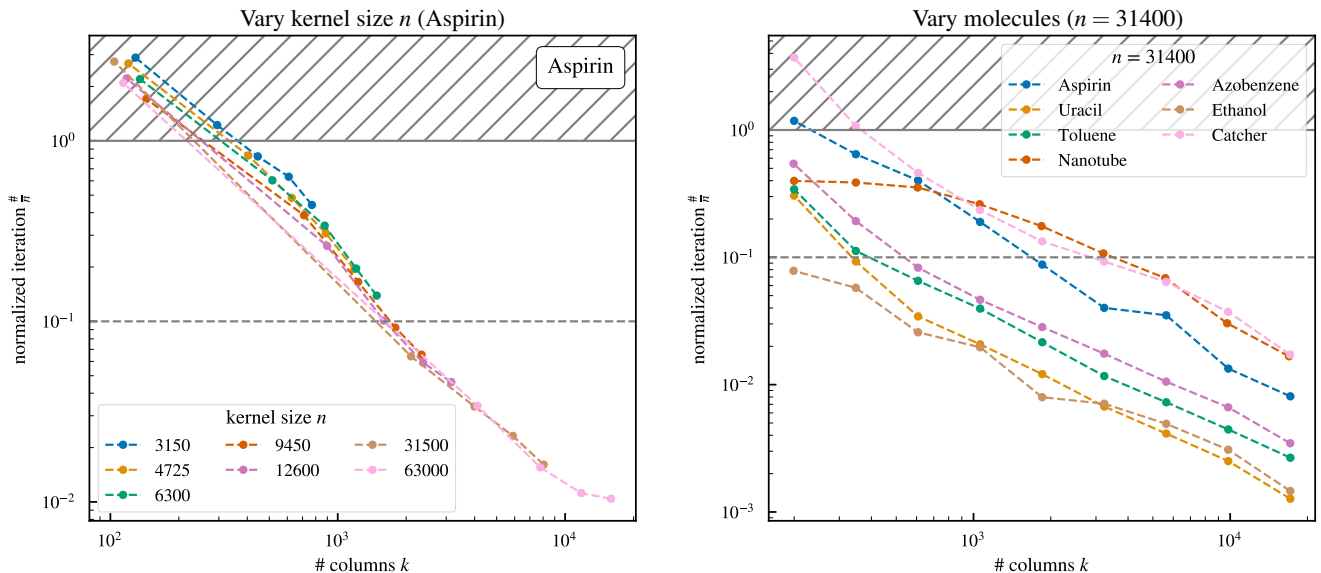


FIG. 6. The super-linear advantage ($\frac{\#}{n} < 1$) of iterative solvers is related to the preconditioning strength k via a monomial power-law (linear dependence in the log-log space). For increasing kernel size n relatively less columns k are needed to obtain an equivalent super-linear advantage. Hence, preconditioners is increasingly valuable (left panel). The monomial trade-off proportionality is verified for any molecule but the exact relation depends on the molecule type (right panel).

TABLE I. Rule of thumb hyperparameters as measured with kernel size $n = 31.400$ (reusing experiments from Figure 6).

	d	m	k_{\min}
Default	—	1	100
Ethanol	9	0.87	10
Uracil	12	1.07	32
Toluene	15	1.01	44
Aspirin	21	1.14	236
Azobenzene	24	1.02	62
Catcher	88	1.02	316
Nanotube	370	0.73	89

too little inducing columns lead to exceedingly long (effectively non-convergent) CG runtimes. Secondly, too many inducing columns are prohibitively costly due to the quadratic k -scaling, which is proportional to the kernel size n . Hence, the optimal preconditioner size k fundamentally scales with the kernel size n , which means that using a fixed (small or large) preconditioner size is clearly not a viable strategy. A naive heuristic is to use a fixed relative ratio of 1% of columns for preconditioning ($k = \frac{n}{100}$)²⁰. In addition, large preconditioners possibly exceed the physical memory and can lead to numerical instabilities.

We derive a more elaborate heuristic based on the overall computational costs of the preconditioned linear solver. These are given by the preconditioner costs $\mathcal{O}(k^2n)$ plus the estimated iterative solver runtime (as formalised by the monomial relation), i.e.,

$$\text{runtime}[k] \propto n^3 \left[\left(\frac{k_{\min}}{k} \right)^m + \left(\frac{k}{n} \right)^2 \right]. \quad (7)$$

Note, that we recover the original cubical runtime for $k \rightarrow k_{\min}$ and $k \rightarrow n$. We then obtain a rule of thumb (RoT) to *predict* the ideal number of columns k^{RoT} for preconditioning via minimizing the overall cost:

$$k^{\text{RoT}} = \min_{k \in [1, n]} \left\{ \text{runtime}[k] \right\} = \left(\frac{(k_{\min})^m m n^2}{2} \right)^{\frac{1}{2+m}}. \quad (8)$$

As discussed in the beginning of this section, both hyperparameters (k_{\min} and m) are connected to spectral properties. Thus, they can be measured for smaller systems and later be reused for larger systems. In Table I we provide estimates for various molecules. We observe, that the slope is consistently close to unity, whereas the minimal preconditioner size k_{\min} is associated with the size of the molecule and its complexity (dominant spectral properties). We define default hyperparameters ($m = 1$, $k_{\min} = 100$) and distinguish between a default vs. a (molecule)-specific RoT.

Experimental validation

We validate our default and specific RoT via measuring the overall runtime depending on the number of inducing columns for various molecules. Thereby, we obtain experimental estimates for the optimal number of inducing columns and the corresponding minimal runtime. We linearly interpolate all measurements to obtain runtime estimates for the default/specific RoT.

In Figure 7 we show the relative runtime between the RoT prediction and the experimental minimum. Additionally, we also compare to the naive baseline of 1% preconditioning ($k = \frac{n}{100}$)²⁰. Interestingly, there are two distinct groups of molecules. Firstly, the small molecules (ethanol, uracil and toluene) for which the naive baseline outperforms our RoT. Secondly, for larger and more complex molecules (aspirin, azobenzene, catcher and nanotube) our RoT is superior. Here, the naive baseline underestimates the preconditioner strength, which leads to severely long (potentially non-convergent) runtimes (plus 18h for the nanotube). Additionally, the RoT can be targeted to a specific molecule type. This further improves the performance of the specific RoT, as compared to its default counterpart. In particular, for all simpler molecules the gap between naive baseline and specific RoT is reduced. Simultaneously, it retains the high performance for the more complex molecules.

All findings are further verified by additional experiments for two smaller kernel sizes ($n = 75000$ and $n = 158000$) in Appendix B 2. Here, the specific RoT is even closer to the experimental minimum, since its molecule-specific parameters (Table I) were estimated using a similar system size ($n = 31400$). This indicates that the specific RoT can be further improved through measuring the hyperparameters for a larger system, i.e., by reducing the gap between estimate and inference kernel size. However, obtaining these more accurate molecule-specific hyperparameters, increases the computational overhead.

Remarks on runtime and predictive accuracy

So far we focused on algorithmic complexities, iterations times and relative solver runtimes. This allowed us to control the important ingredients which dominate the overall runtime. Firstly, the kernel size n (which we kept fix when comparing different molecules) and secondly, the molecule complexity, as encoded in its spectrum. We now discuss the nominal runtimes as stated in the molecule label of Figure 7. For example, the runtime of uracil is one order of magnitude smaller as compared to the nanotube molecule. This roughly agrees with their relative difference (based on CG iteration time) in Figure 6 (right panel). Indeed, we find a good agreement between the ordering in terms of iteration steps (Figure 6) and actual experimental runtimes (Figure 7). For example consider uracil and ethanol, which are consistently the simplest molecules to solve. Alternatively, the most expensive molecules are the catcher and nanotube molecules. Interestingly, from Figure 6 (right panel) we deduce that their runtime should be identi-

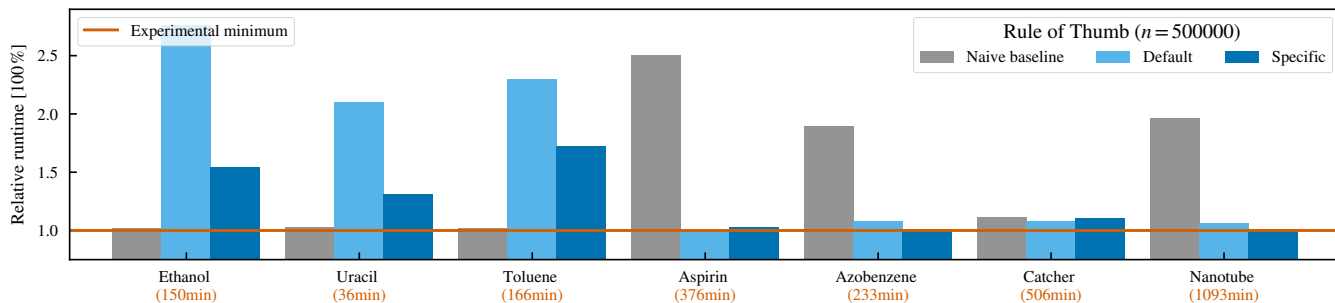


FIG. 7. Minimizing the overall runtime by estimating the ideal number of inducing columns k in advance. All runtimes are given as relative percentage of experimental optimal runtime (orange), which is stated in parentheses. Fixed kernel size $n = 500000$ (see Appendix B for smaller kernel sizes). The rule of thumb is superior for complex and difficult to converge molecules, e.g. catcher or nanotube. For simpler and fast converging molecules (ethanol or uracil) a molecule specific rule of thumb can reduce the gap wrt. the naive baseline estimate (fixed $k = 1\% \cdot n$ preconditioner strength).

cal. However, the experimental nanotube runtime is twice as long as for the catcher molecule. This effect is closely related to the sGDML approach, which by construction builds on the molecule size d (cf. Section III A). This is why larger molecules are computationally more demanding.

Lastly, we compare the nominal runtimes and accuracies between a standard analytic (closed-form) solver and the preconditioned CG solver using the ideal number of inducing columns as predicted by our specific RoT. The results in Table II show no significant differences in the accuracy of the force prediction. However, iterative solver is up to 5x faster as compared to its analytic (closed-form) counterpart. Hence, the preconditioned CG solver enables state of the art FF predictions at lower computational costs, both in terms of runtime as well as memory. We emphasize that the kernel size was limited to $n = 63000$ (matching 1000 aspirin points) due to constraining analytic solver, which needs access to the complete kernel matrix ($\sim 30\text{GB}$). In contrast, the preconditioned CG only requires to store a smaller preconditioner ($\sim 3\text{GB}$) and thus allows to scale to much larger problem sizes (as done in Figure 7). Note, that the cost for computing the preconditioner are negligible for a small number of inducing columns and hence preconditioned iterative solvers are effectively always superior to closed-form solvers for large systems²⁴.

Overall, we conclude that our proposed heuristic provides an accurate and robust estimate for a practically well-performing number of inducing columns. This circumvents unnecessary large or too small preconditioners and can thus substantially speed-up training. Our default RoT provides reasonable estimates irrespective of molecule type and kernel size. Moreover, we demonstrated that our approach can be targeted to a specific molecule type and is therefore extendable to new molecules.

V. CONCLUSION

To enable large scale kernel learning for quantum chemistry this study proposes a combination of Nyström preconditioner and CG solver. We establish a fundamental trade off using this combination: Physical correlations give rise to exceedingly

TABLE II. Comparing accuracy (mean-absolute error (MAE) of force prediction in $\text{mol kcal}^{-1} \text{\AA}^{-1}$) and runtime between the analytic (closed-form) and preconditioned CG (PCG) solver for a fixed kernel size $n = 63000$. Experiments were performed on a NVIDIA A100 (40GB). The PCG performs indistinguishably at faster runtimes and lower memory demand.

Molecule	Accuracy	Runtime [min]		
	$ \text{MSE}_{\text{PCG}} - \text{MSE}_{\text{Analytic}} $	Analytic	PCG	Speed-up
Ethanol	0.00003	38 ± 8	10.5 ± 1.6	$3.6\times$
Uracil	0.00007	33 ± 10	6.5 ± 0.6	$5.0\times$
Toluene	0.00002	41 ± 10	11.2 ± 1.7	$3.6\times$
Aspirin	0.00006	35 ± 8	25.3 ± 3.1	$1.4\times$
Azobenzene	0.00012	35 ± 10	12.0 ± 2.1	$2.9\times$
Catcher	0.00009	50 ± 13	50.4 ± 6.0	$1.0\times$
Nanotube	0.00002	151 ± 44	70 ± 12	$2.2\times$

ill-conditioned loss surfaces, which can be readily addressed by selecting the appropriate inducing columns. Whereas, the remaining stochasticity of the learning problem can be targeted with the Krylov subspace spanned by the iterative CG solver. Both together can be viewed as a low-rank expansion, which allows for a chemically interpretation in terms of molecular fragments. This means that given a Nyström preconditioner, the CG’s super-linear convergence coincides with the number of inducing columns k and not kernel size n . Using these insights, we derived an intuitive heuristic to balance this trade off and to infer a practically well-performing preconditioner strength in advance. Overall, we verify close to experimentally optimal runtimes for various molecules and different problem sizes. Importantly, our rule of thumb generalizes as it can be targeted to new molecules.

Moreover, we discovered interesting differences and commonalities when comparing inducing column selection strategies that are representative for a wide spectrum of preconditioner construction techniques. For simpler molecules it

suffices to uniformly sample inducing columns and thereby construct a scalable kernel solver. In contrast, for more involved physical systems the situation is more challenging, as the relevant information is unevenly distributed. Hence, naive approaches are not sufficient and lack the essential physical ingredients. In our case, the incomplete Cholesky decomposition is able to incorporate the dominant signals from the complex catcher or nanotube molecules to construct a diverse, representative set of inducing columns. In turn, this leads to superior preconditioner performance. Generally, for other challenging domains, such as biomedical molecules or materials, there are rich physical structures which can be unravelled to build more efficient learning algorithms.

ACKNOWLEDGEMENTS

The authors have no conflicts to disclose. SB, SC and KRM acknowledge support by the German Federal Ministry of Education and Research (BMBF) for BIFOLD (01IS18037A). KRM was partly supported by the Institute of Information & Communications Technology Planning & Evaluation (IITP) grants funded by the government (MSIT) (No. 2019-0-00079, Artificial Intelligence Graduate School Program, Korea University and No. 2022-0-00984, Development of Artificial Intelligence Technology for Personalized Plug-and-Play Explanation and Verification of Explanation) and by the German Federal Ministry for Education and Research (BMBF) under Grants 01IS14013B-E, 01GQ1115.

Appendix A: Technical details

1. SVD preconditioner

The singular-value decomposition (SVD) provides access to the optimal low-rank approximation of K . Since K is PSD the SVD is equivalent to the eigendecomposition, i.e. all left- and right-singular vectors are identical. The SVD is given by

$$K = U \Sigma U^T, \quad (\text{A1})$$

with U being a unitary matrix consisting of all eigenvectors $[\mathbf{u}_1, \dots, \mathbf{u}_n]$ and the diagonal matrix of singular values $\Sigma = \text{diag}(\sqrt{\lambda_1}, \dots, \sqrt{\lambda_n})$. An optimal rank- k SVD preconditioner is based on the k dominant eigendirections, leading to the rank- k approximation $K_k = U_k \Sigma_k U_k^T$. Importantly, this approach directly targets the dominant eigenvectors and explicitly removes their effect from the spectrum. In this sense, the SVD preconditioner optimally flattens the kernel spectrum. Unfortunately, calculating the SVD scales quadratic with the kernel size $\mathcal{O}(kn^2)$ and therefore offers little practical value. However, for small system SVD preconditioning is computationally feasible and we can use it as an theoretical lower bound for practical preconditioners.

Preconditioned CG as low-rank solver The solution of the linear system Equation (1) can be expressed by the span of all non-trivial (i.e. up to the λ -regularized null space $l \approx 6n_{\text{train}}$) kernel eigenvectors $\boldsymbol{\alpha} \in \text{span}[\mathbf{u}_0, \dots, \mathbf{u}_l]$. A CG solver expresses this solution iteratively within a Krylov basis $\mathcal{P} = \{p_1, \dots, p_{\#}\}$, which approximates the complete spectrum simultaneously (hence $\text{span}[\mathcal{P}] \approx \text{span}[K_{\lambda}]$ after convergence). For example consider a flat spectrum spectrum (e.g. a fully preconditioned system), the CG converges in a single iterations, i.e. all $[\mathbf{u}_1, \dots, \mathbf{u}_l]$ eigenvectors are summarized by a single search direction \mathbf{p}_1 . In contrast, for an ill-conditioned learning problem (maximally non-uniform spectrum) the CG requires many iterations to converge. However, using $\# = l$ search directions we are guaranteed to recover the correct spectrum ($\text{span}[\mathcal{P}] = \text{span}[K_{\lambda}]$) and the approach becomes exact.

We can now interpolate between both extremes using a preconditioner (Equation (2)). A preconditioner can directly target the dominant eigenvectors and partially remove (pre-solve) the challenging physical eigenvectors. Hence, the resulting preconditioned linear system is characterised by $\text{span}[(K_k + \lambda I_n)^{-1} K_{\lambda}] = \text{span}[\mathbf{u}_{k+1}, \dots, \mathbf{u}_l] \approx \text{span}[\mathcal{P}]$ and overall the solution is expressed by two linear independent sets of basis vectors

$$\boldsymbol{\alpha} \in \text{span}[\mathbf{u}_1, \dots, \mathbf{u}_k] + \text{span}[\mathbf{p}_1, \dots, \mathbf{p}_{\#}]. \quad (\text{A2})$$

As we showed in Section IV C, it is possible to tune preconditioner size k such that $k + \# \ll n$ and thereby construct an efficient low-rank decomposition of the kernel.

Atomic contribution To intuitively visualize the low-rank decomposition defined by the SVD, we derive individual atomic contributions for each eigenvectors \mathbf{u}_i . To this end, we reshape each n -dimensional eigenvector into its individual components: $n \mapsto (n_{\text{train}}, d, 3)$. Due to the periodicity within

the structured eigenvectors (as discussed in Section II A), we can average over the training dimension. Lastly, we measure the L2 distance wrt. the remaining three spatial dimensions to obtain a d -dimensional atomic contribution for each eigenvector.

2. Incomplete Cholesky decomposition

To facilitate reproducibility, we provide pseudo code for an efficient incomplete Cholesky decomposition in Algorithm 1. Importantly, this algorithm only requires access to pivot columns and the kernel trace. Additionally, it does not require to compute the full Schur complement S . Thereby, it achieves minimal runtime $\mathcal{O}(k^2 n)$ and memory $\mathcal{O}(kn)$ cost.

Algorithm 1: incomplete Cholesky decomposition
optimized for NUMPY, adapted from⁷⁰

```

Input : function: get_col( $i$ )  $\mapsto \mathbf{k}_i \in \mathbb{R}^n$ ,
         array:  $\mathbf{d} := \text{diag}(K) \in \mathbb{R}^n$ ,
         int:  $k \leq n$ 
Output : array:  $L_k := [l_{i,m}] \in \mathbb{R}^{n \times k}$ 
1 begin
2   initialize  $\boldsymbol{\pi} := (1, 2, \dots, n)$ 
3   initialize  $L_k := \text{zeros}(n, k)$ 
4   for  $1 \leq m \leq k$  do
5     // Find pivot in permuted diagonal
5     set  $i := \arg \max \{d_{\pi_j} : j = m, m+1, \dots, n\}$ 
6     swap  $\pi_m$  and  $\pi_i$ 
7     define  $\boldsymbol{\pi}_{>m} := (\pi_j : j = m+1, \dots, n)$ 
8     // Set pivot and get new column
8     set  $l_{\pi_m, m} := \sqrt{d_{\pi_m}}$ 
9     set  $\mathbf{k}_m = \text{get\_col}(\pi_m)$ 
10    // Calculate Schur correction
10    // use np.einsum
10     $\mathbf{s} := \sum_{j=1}^m l_{\pi_m, j} \cdot l_{\boldsymbol{\pi}_{>m}, j}$  //  $\text{len}(\mathbf{s}) = n - m$ 
11    set  $l_{\boldsymbol{\pi}_{>m}, m} := (\mathbf{k}_{\boldsymbol{\pi}_{>m}} - \mathbf{s}) / l_{\pi_m, m}$ 
11    // Update diagonal
12     $d_{\boldsymbol{\pi}_{>m}} = d_{\boldsymbol{\pi}_{>m}} - l_{\boldsymbol{\pi}_{>m}, m}^2$ 
13  end
14  return  $L_k$ 
15 end

```

Appendix B: Experimental results for more molecules

1. Preconditioned spectra

Jacobi preconditioning is a simple and often effective alternative^{71–74}. It assumes a *local* block-dominant matrix structure. In principle, it is therefore able to incorporate all structured prototype eigenvectors. To experimentally show the necessity to incorporate global correlations, we show the effective spectra for local preconditioners in Figure 8. Firstly, we simply approximate the kernel matrix K by a block-diagonal matrix (*naive Jacobi* preconditioning). As expected, since the kernel matrix is not block dominant, this

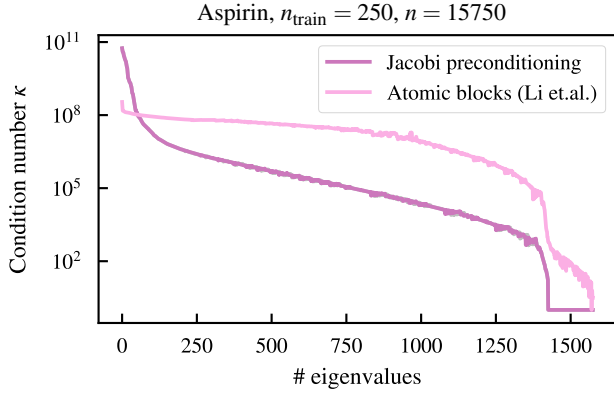


FIG. 8. The effective spectrum of $P^{-1}K$ for simple Jacobi preconditioning and advanced atomic-block preconditioning¹⁸. The local structure prohibits to reduce the condition number sufficiently for practical usage as a preconditioner.

approach does not improve the conditioning. Secondly, we consider keep all correlations between identical atoms and zero out all other remaining structure. This generates a permuted block structure, which can be used as a platform for (*advanced atomic-block* (Jacobi) preconditioning. This physically motivated atomic-block approximation was proposed for approximative inference in¹⁸. However, this approach only mildly flattens the spectrum and is hence insufficient for practical preconditioning. This fundamentally relates to the fact that kernel matrices describe correlations between all training points, which can not be truncated.

Additionally, we provide preconditioned **spectra for more molecules** in Figure 9. As discussed in the main body of this manuscript, the incomplete Cholesky preforms nearly optimal for small number of inducing columns. However, for larger k all practical preconditioner perform interchangeably.

2. Convergence of conjugate gradient

In Figure 10 we show the convergence for more molecules and further validate our findings described in the main text. As previously observed, all inducing column based preconditioners are similarly effective for most molecules and lower bounded the optimal SVD preconditioner.

To further investigate the unexpected differences between random and leverage score based columns sampling, we consider an additional variant of the latter, namely rank- k leverage scores⁷⁵:

$$\tau_i(K_k) = |[U_k]_{i,:}|_2^2. \quad (\text{B1})$$

Here, $[U_k]_{i,:}$ denotes the i -th row of U_k . The sub-dominant spectral directions are diminish via omitting the corresponding eigenvectors. This allows to directly match the rank- k for the leverage scores estimation to the preconditioner size k . Thereby, the rank- k leverage scores adapt to the changing dimensionality of preconditioner subspace. This is in contrast to ridge leverage scores: Here, sub-dominant spectral dimensions were suppressed by a regularization λ , which was

matched to the overall ridge regularization from Equation (1). Thereby, ridge leverage scores are indicative for a fixed regularized kernel spectrum. Lastly, we emphasize that this definition of rank- k leverage scores requires to calculate the SVD decomposition and is therefore too expensive for practical usability. One possibility would be to use ridge leverage scores with an adaptive regularization λ as induced by the requested preconditioner size k ⁶⁸.

The experimental results in Figure 10 show that the improved rank- k leverage scores bridge the gap to the performance of uniform sampling, as observed for the catcher and nanotube molecule. However, there are no significant differences between both approaches and both are clearly lower-bounded by the incomplete Cholesky column selection strategy.

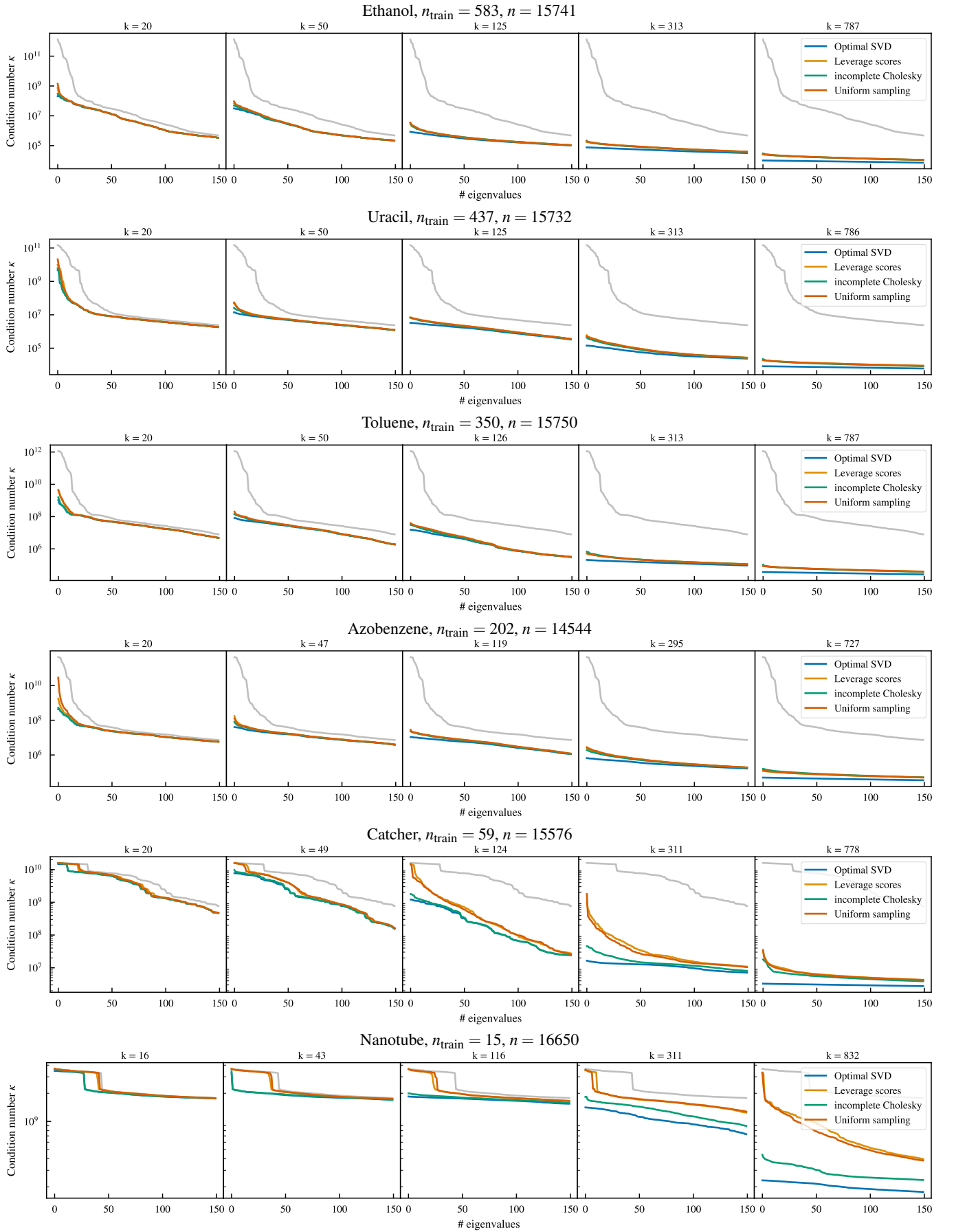


FIG. 9. Preconditioned spectrum of $P^{-1}K$ for varying preconditioner size k (restricted to the dominant 150 eigenvalues).

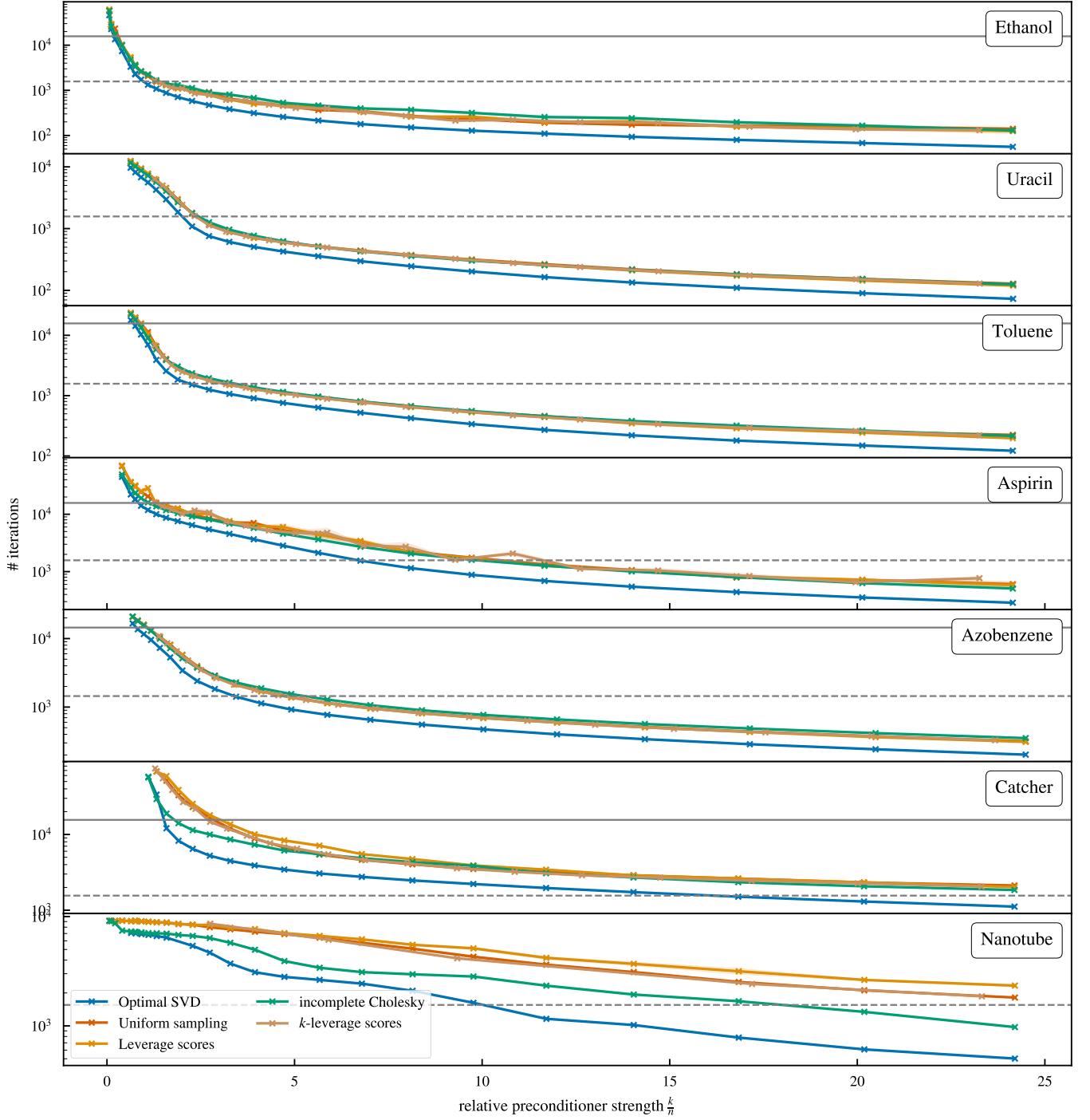


FIG. 10. Iterative convergence speed for varying preconditioner strength for fixed kernel size $n \approx 15000$ ($n_{\text{train}} = 250$ for aspirin). Only minor performance differences are visible for ethanol. In contrast, for more complex molecules (catcher, nanotube) the elaborate incomplete Cholesky preconditioner is superior to naive random sampling of inducing columns.

Appendix C: Rule of thumb

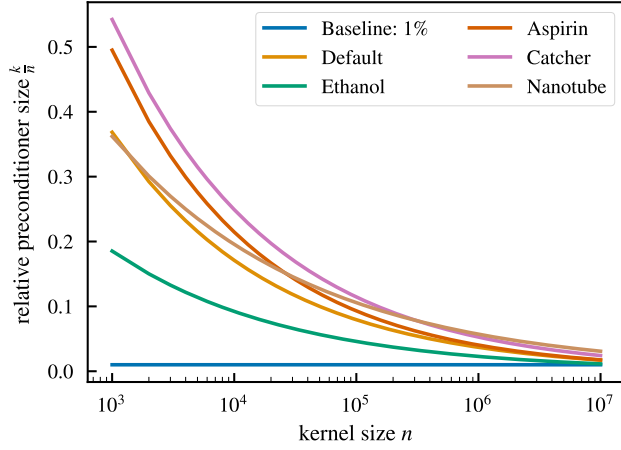


FIG. 11. Comparing the predicted preconditioner size of all used heuristics depending on the kernel size n .

We experimentally validate our heuristic rule of thumb for two additional, smaller kernel sizes in Figure 12. To corresponding hardware specification are summarized in Table III. For the readers convenience we compare the prediction for all heuristics (default/specific RoT, naive baseline) depending on the kernel size n in Figure 11. In contrast to the naive baseline, our RoT adapts to the kernel size n and is therefore applicable over several orders of magnitude.

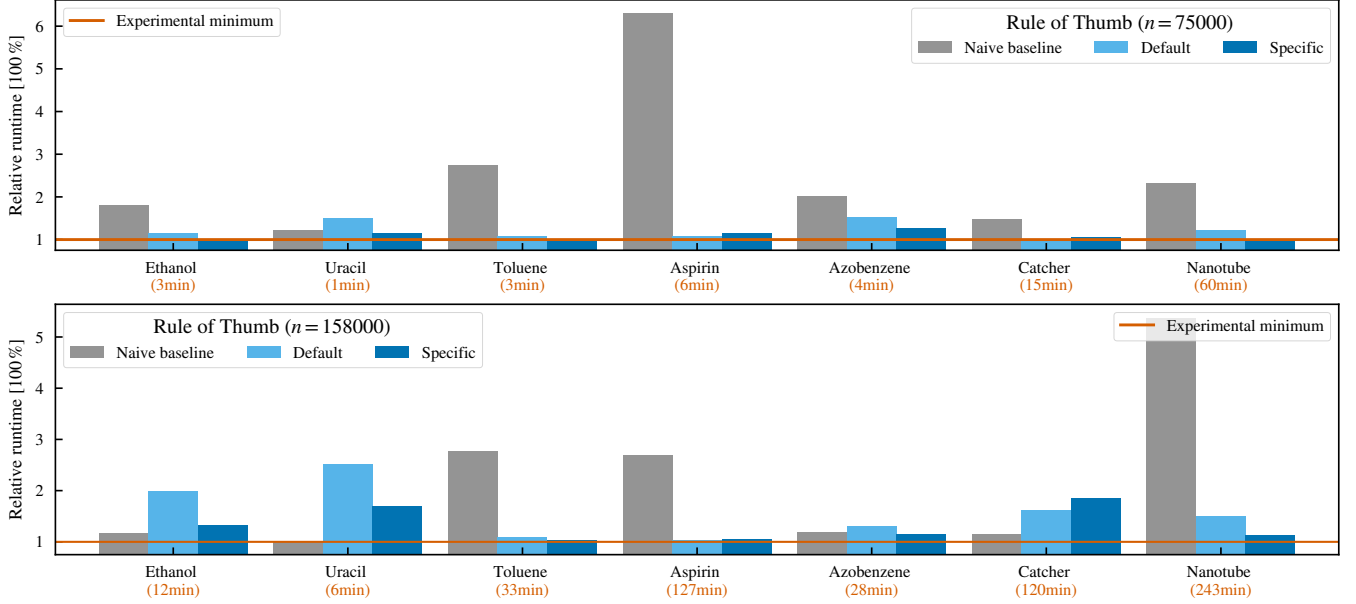


FIG. 12. Experimental validation of the rule of thumb for various molecules and fixed kernel size $n = 75,000$ and $n = 158,000$. The minimal runtime is printed in parentheses.

TABLE III. Hardware specification used for the RoT validation experiments (Figure 7 and 12).

n	Ethanol	Uracil	Toluene	Aspirin
75000	CPU Gold 6226R	Gold 6226R	Gold 6226R	Gold 6226R
	GPU Quadro RTX 6000 (24GB)	Quadro RTX 6000 (24GB)	A100 (40GB)	Quadro RTX 6000 (24GB)
157500	CPU Gold 6226R	Gold 6226R	E5-2690 v4	E5-2690 v4
	GPU A100 (40GB)	A100 (40GB)	P100 (12GB)	P100 (12GB)
504000	CPU Gold 6226R	Gold 6226R	Gold 6226R	Gold 6226R
	GPU A100 (40GB)	Quadro RTX 6000 (24GB)	A100 (40GB)	Quadro RTX 6000 (24GB)
n	Azobenzene	Catcher	Nanotube	
75000	CPU Gold 6226R	Gold 6226R	E5-2650 v4	
	GPU Quadro RTX 6000 (24GB)	A100 (80GB)	TITAN RTX (24GB)	
157500	CPU Gold 6226R	E5-2690 v4	Gold 6226R	
	GPU A100 (40GB)	P100 (12GB)	A100 (40GB)	
504000	CPU Gold 6226R	Gold 6226R	Gold 6226R	
	GPU Quadro RTX 6000 (24GB)	A100 (40GB)	Quadro RTX 6000 (24GB)	

- ¹F. Noé, A. Tkatchenko, K.-R. Müller, and C. Clementi, "Machine learning for molecular simulation," *Annual review of physical chemistry* **71**, 361–390 (2020).
- ²O. T. Unke, S. Chmiela, H. E. Sauceda, M. Gastegger, I. Poltavskyi, K. T. Schütt, A. Tkatchenko, and K.-R. Müller, "Machine learning force fields," *Chemical Reviews* **121**, 10142–10186 (2021).
- ³J. A. Keith, V. Vassilev-Galindo, B. Cheng, S. Chmiela, M. Gastegger, K.-R. Müller, and A. Tkatchenko, "Combining machine learning and computational chemistry for predictive insights into chemical systems," *Chemical reviews* **121**, 9816–9872 (2021).
- ⁴J. Behler and M. Parrinello, "Generalized neural-network representation of high-dimensional potential-energy surfaces," *Physical Review Letters* **98**, 146401 (2007).
- ⁵J. Behler, "Atom-centered symmetry functions for constructing high-dimensional neural network potentials," *The Journal of Chemical Physics* **134**, 074106 (2011).
- ⁶J. T. Frank, O. T. Unke, and K.-R. Müller, "So3krates: Equivariant attention for interactions on arbitrary length-scales in molecular systems," *Advances in Neural Information Processing Systems* **35** (2022).
- ⁷N. Lubbers, J. S. Smith, and K. Barros, "Hierarchical modeling of molecular energies using a deep neural network," *The Journal of Chemical Physics* **148**, 241715 (2018).
- ⁸K. T. Schütt, F. Arbabzadah, S. Chmiela, K. R. Müller, and A. Tkatchenko, "Quantum-chemical insights from deep tensor neural networks," *Nature Communications* **8**, 13890 (2017).
- ⁹O. T. Unke and M. Meuwly, "Physnet: A neural network for predicting energies, forces, dipole moments, and partial charges," *Journal of Chemical Theory and Computation* **15**, 3678–3693 (2019).
- ¹⁰O. T. Unke, S. Chmiela, M. Gastegger, K. T. Schütt, H. E. Sauceda, and K.-R. Müller, "Spookynet: Learning force fields with electronic degrees of freedom and nonlocal effects," *Nature Communications* **12**, 7273 (2021).
- ¹¹M. Rupp, A. Tkatchenko, K.-R. Müller, and O. A. Von Lilienfeld, "Fast and accurate modeling of molecular atomization energies with machine learning," *Physical Review Letters* **108**, 058301 (2012).
- ¹²S. Chmiela, H. E. Sauceda, K.-R. Müller, and A. Tkatchenko, "Towards exact molecular dynamics simulations with machine-learned force fields," *Nature Communications* **9**, 3887 (2018).
- ¹³S. Chmiela, H. E. Sauceda, I. Poltavsky, K.-R. Müller, and A. Tkatchenko, "sgdml: Constructing accurate and data efficient molecular force fields using machine learning," *Computer Physics Communications* **240**, 38–45 (2019).
- ¹⁴A. S. Christensen, L. A. Bratholm, F. A. Faber, and O. Anatole von Lilienfeld, "Fchl revisited: Faster and more accurate quantum machine learning," *The Journal of Chemical Physics* **152**, 044107 (2020).
- ¹⁵V. L. Deringer, A. P. Bartók, N. Bernstein, D. M. Wilkins, M. Ceriotti, and G. Csányi, "Gaussian process regression for materials and molecules," *Chemical Reviews* **121**, 10073–10141 (2021).
- ¹⁶F. A. Faber, A. S. Christensen, B. Huang, and O. A. Von Lilienfeld, "Alchemical and structural distribution based representation for universal quantum machine learning," *The Journal of Chemical Physics* **148**, 241717 (2018).
- ¹⁷A. Glielmo, P. Sollich, and A. De Vita, "Accurate interatomic force fields via machine learning with covariant kernels," *Physical Review B* **95**, 214302 (2017).
- ¹⁸H. Li, M. Zhou, J. Sebastian, J. Wu, and M. Gu, "Efficient force field and energy emulation through partition of permutationally equivalent atoms," *The Journal of Chemical Physics* **156**, 184304 (2022).
- ¹⁹H. E. Sauceda, L. E. Gálvez-González, S. Chmiela, L. O. Paz-Borbón, K.-R. Müller, and A. Tkatchenko, "Bigdml—towards accurate quantum machine learning force fields for materials," *Nature Communications* **13**, 3733 (2022).
- ²⁰S. Chmiela, V. Vassilev-Galindo, O. T. Unke, A. Kabylda, H. E. Sauceda, A. Tkatchenko, and K.-R. Müller, "Accurate global machine learning force fields for molecules with hundreds of atoms," *arXiv preprint arXiv:2209.14865* (2022).
- ²¹C. Chen, Z. Deng, R. Tran, H. Tang, I.-H. Chu, and S. P. Ong, "Accurate force field for molybdenum by machine learning large materials data," *Physical Review Materials* **1**, 043603 (2017).
- ²²Y. Zhang and C. Ling, "A strategy to apply machine learning to small datasets in materials science," *Npj Computational Materials* **4**, 25 (2018).
- ²³O. T. Unke, M. Stöhr, S. Gansch, T. Unterthiner, H. Maennel, S. Kashubin, D. Ahlin, M. Gastegger, L. M. Sandomas, A. Tkatchenko, *et al.*, "Accurate machine learned quantum-mechanical force fields for biomolecular simulations," *arXiv preprint arXiv:2205.08306* (2022).
- ²⁴J. Gardner, G. Pleiss, K. Q. Weinberger, D. Bindel, and A. G. Wilson, "Gpytorch: Blackbox matrix-matrix gaussian process inference with gpu acceleration," *Advances in Neural Information Processing Systems* **31** (2018).
- ²⁵H. Liu, Y.-S. Ong, X. Shen, and J. Cai, "When gaussian process meets big data: A review of scalable gps," *IEEE Transactions on Neural Networks and Learning systems* **31**, 4405–4423 (2020).
- ²⁶K. Wang, G. Pleiss, J. Gardner, S. Tyree, K. Q. Weinberger, and A. G. Wilson, "Exact gaussian processes on a million data points," *Advances in Neural Information Processing Systems* **32** (2019).
- ²⁷N. F. Schmitz, K.-R. Müller, and S. Chmiela, "Algorithmic differentiation for automated modeling of machine learned force fields," *The Journal of Physical Chemistry Letters* **13**, 10183–10189 (2022).
- ²⁸C. Williams and M. Seeger, "Using the nystrom method to speed up kernel machines," *Advances in Neural Information Processing Systems* **13** (2000).
- ²⁹R. Patel, T. Goldstein, E. Dyer, A. Mirhoseini, and R. Baraniuk, "Deterministic column sampling for low-rank matrix approximation: Nystrom vs. incomplete cholesky decomposition," in *International Conference on Data Mining* (SIAM, 2016) pp. 594–602.
- ³⁰S. Kumar, M. Mohri, and A. Talwalkar, "Sampling techniques for the nystrom method," in *International Conference on Artificial Intelligence and Statistics* (PMLR, 2009) pp. 304–311.
- ³¹C. Musco and C. Musco, "Recursive sampling for the nystrom method," *Advances in Neural Information Processing Systems* **30** (2017).
- ³²S. Chmiela, A. Tkatchenko, H. E. Sauceda, I. Poltavsky, K. T. Schütt, and K.-R. Müller, "Machine learning of accurate energy-conserving molecular force fields," *Science advances* **3**, e1603015 (2017).
- ³³N. Freitas, Y. Wang, M. Mahdavian, and D. Lang, "Fast krylov methods for n-body learning," *Advances in Neural Information Processing Systems* **18** (2005).
- ³⁴M. R. Hestenes and E. Stiefel, "Methods of conjugate gradients for solving linear systems," *Journal of Research of the National Bureau of Standards* **49**, 409 (1952).
- ³⁵K. I. Kim, M. O. Franz, and B. Schölkopf, "Iterative kernel principal component analysis for image modeling," *IEEE Transactions on Pattern Analysis and Machine Intelligence* **27**, 1351–1366 (2005).
- ³⁶B. V. Srinivasan, Q. Hu, N. A. Gumerov, R. Murtugudde, and R. Duraiswami, "Preconditioned krylov solvers for kernel regression," *arXiv preprint arXiv:1408.1237* (2014).
- ³⁷A. Rudi, L. Carratino, and L. Rosasco, "Falkon: An optimal large scale kernel method," *Advances in Neural Information Processing Systems* **30** (2017).
- ³⁸W. Hackbusch, *Iterative solution of large sparse systems of equations*, Vol. 95 (Springer, 1994).
- ³⁹Y. Saad, *Iterative methods for sparse linear systems* (SIAM, 2003).
- ⁴⁰A. Van der Sluis and H. A. van der Vorst, "The rate of convergence of conjugate gradients," *Numerische Mathematik* **48**, 543–560 (1986).
- ⁴¹O. Axelsson and I. Kaporin, "On the sublinear and superlinear rate of convergence of conjugate gradient methods," *Numerical Algorithms* **25**, 1–22 (2000).
- ⁴²B. Beckermann and A. B. Kuijlaars, "Superlinear convergence of conjugate gradients," *SIAM Journal on Numerical Analysis* **39**, 300–329 (2001).
- ⁴³M. L. Braun, J. M. Buhmann, and K.-R. Müller, "On relevant dimensions in kernel feature spaces," *The Journal of Machine Learning Research* **9**, 1875–1908 (2008).
- ⁴⁴H. Avron, K. L. Clarkson, and D. P. Woodruff, "Faster kernel ridge regression using sketching and preconditioning," *SIAM Journal on Matrix Analysis and Applications* **38**, 1116–1138 (2017).
- ⁴⁵M. Benzi, "Preconditioning techniques for large linear systems: a survey," *Journal of Computational Physics* **182**, 418–477 (2002).
- ⁴⁶K. Cutajar, M. Osborne, J. Cunningham, and M. Filippone, "Preconditioning kernel matrices," in *International Conference on Machine Learning* (PMLR, 2016) pp. 2529–2538.
- ⁴⁷E. F. Kaasschieter, "Preconditioned conjugate gradients for solving singular systems," *Journal of Computational and Applied Mathematics* **24**, 265–275 (1988).

- ⁴⁸S. Ma and M. Belkin, “Diving into the shallows: a computational perspective on large-scale shallow learning,” *Advances in Neural Information Processing Systems* **30** (2017).
- ⁴⁹G. Shabat, E. Choshen, D. B. Or, and N. Carmel, “Fast and accurate gaussian kernel ridge regression using matrix decompositions for preconditioning,” *SIAM Journal on Matrix Analysis and Applications* **42**, 1073–1095 (2021).
- ⁵⁰T. Zhou and D. Tao, “Godec: Randomized low-rank & sparse matrix decomposition in noisy case,” in *Proceedings of the 28th International Conference on Machine Learning, ICML 2011* (2011).
- ⁵¹W. B. Johnson, “Extensions of lipschitz mappings into a hilbert space,” *Contemporary Mathematics* **26**, 189–206 (1984).
- ⁵²N. Halko, P.-G. Martinsson, and J. A. Tropp, “Finding structure with randomness: Probabilistic algorithms for constructing approximate matrix decompositions,” *SIAM review* **53**, 217–288 (2011).
- ⁵³C. Li, S. Jegelka, and S. Sra, “Fast dpp sampling for nystrom with application to kernel methods,” in *International Conference on Machine Learning* (PMLR, 2016) pp. 2061–2070.
- ⁵⁴S. Sun, J. Zhao, and J. Zhu, “A review of nystrom methods for large-scale machine learning,” *Information Fusion* **26**, 36–48 (2015).
- ⁵⁵A. J. Smola and B. Schölkopf, “Sparse greedy matrix approximation for machine learning,” in *International Conference on Machine Learning* (Morgan Kaufmann, 2000) pp. 911–918.
- ⁵⁶P. Drineas, M. W. Mahoney, and N. Cristianini, “On the nystrom method for approximating a gram matrix for improved kernel-based learning,” *The Journal of Machine Learning Research* **6**, 2153–2175 (2005).
- ⁵⁷K. Zhang, I. W. Tsang, and J. T. Kwok, “Improved nystrom low-rank approximation and error analysis,” in *International Conference on Machine Learning* (2008) pp. 1232–1239.
- ⁵⁸H. Al Daas, T. Rees, and J. Scott, “Two-level nystrom- schur preconditioner for sparse symmetric positive definite matrices,” *SIAM Journal on Scientific Computing* **43**, A3837–A3861 (2021).
- ⁵⁹Z. Frangella, J. A. Tropp, and M. Udell, “Randomized nystrom preconditioning,” *arXiv preprint arXiv:2110.02820* (2021).
- ⁶⁰H. Kim and Y. W. Teh, “Scaling up the automatic statistician: Scalable structure discovery using gaussian processes,” in *International Conference on Artificial Intelligence and Statistics* (PMLR, 2018) pp. 575–584.
- ⁶¹L. Foster, A. Waagen, N. Aijaz, M. Hurley, A. Luis, J. Rinsky, C. Satyavolu, M. J. Way, P. Gazis, and A. Srivastava, “Stable and efficient gaussian process calculations,” *The Journal of Machine Learning Research* **10** (2009).
- ⁶²F. Bach, “Sharp analysis of low-rank kernel matrix approximations,” in *Conference on learning theory* (PMLR, 2013) pp. 185–209.
- ⁶³M. B. Cohen, Y. T. Lee, C. Musco, C. Musco, R. Peng, and A. Sidford, “Uniform sampling for matrix approximation,” in *Conference on Innovations in Theoretical Computer Science* (2015) pp. 181–190.
- ⁶⁴A. Gittens and M. W. Mahoney, “Revisiting the nystrom method for improved large-scale machine learning,” *The Journal of Machine Learning Research* **17**, 3977–4041 (2016).
- ⁶⁵I. C. Ipsen and T. Wentworth, “Sensitivity of leverage scores,” *arXiv preprint arXiv:1402.0957* (2014).
- ⁶⁶S. Wang and Z. Zhang, “Improving cur matrix decomposition and the nystrom approximation via adaptive sampling,” *The Journal of Machine Learning Research* **14**, 2729–2769 (2013).
- ⁶⁷A. Alaoui and M. W. Mahoney, “Fast randomized kernel ridge regression with statistical guarantees,” *Advances in Neural Information Processing Systems* **28** (2015).
- ⁶⁸S. McCurdy, “Ridge regression and provable deterministic ridge leverage score sampling,” *Advances in Neural Information Processing Systems* **31** (2018).
- ⁶⁹S. Fine and K. Scheinberg, “Efficient svm training using low-rank kernel representations,” *The Journal of Machine Learning Research* **2**, 243–264 (2001).
- ⁷⁰H. Harbrecht, M. Peters, and R. Schneider, “On the low-rank approximation by the pivoted cholesky decomposition,” *Applied Numerical Mathematics* **62**, 428–440 (2012).
- ⁷¹H. Anzt, J. Dongarra, G. Flegar, N. J. Higham, and E. S. Quintana-Ortí, “Adaptive precision in block-jacobi preconditioning for iterative sparse linear system solvers,” *Concurrency and Computation: Practice and Experience* **31**, e4460 (2019).
- ⁷²P. Concus, G. H. Golub, and G. Meurant, “Block preconditioning for the conjugate gradient method,” *SIAM Journal on Scientific and Statistical Computing* **6**, 220–252 (1985).
- ⁷³A. V. Knyazev, “Toward the optimal preconditioned eigensolver: Locally optimal block preconditioned conjugate gradient method,” *SIAM Journal on Scientific Computing* **23**, 517–541 (2001).
- ⁷⁴F.-H. Lee, K.-K. Phoon, K. Lim, and S. Chan, “Performance of jacobi preconditioning in krylov subspace solution of finite element equations,” *International Journal for Numerical and Analytical Methods in Geomechanics* **26**, 341–372 (2002).
- ⁷⁵D. Papailiopoulos, A. Kyriillidis, and C. Boutsidis, “Provable deterministic leverage score sampling,” in *Proceedings of the 20th ACM SIGKDD international conference on Knowledge discovery and data mining* (2014) pp. 997–1006.